Core-level photoabsorption study of defects and metastable bonding configurations in boron nitride

I. Jiménez,* A. F. Jankowski, L. J. Terminello, D. G. J. Sutherland, and J. A. Carlisle
Lawrence Livermore National Laboratory, Livermore, California 94551

G. L. Doll
Materials Research Department, Timken Research, Canton, Ohio 44706

W. M. Tong and D. K. Shuh
Lawrence Berkeley National Laboratory, Berkeley, California 94720

F. J. Himpsel
Department of Physics, University of Wisconsin-Madison, Madison, Wisconsin 53706

(Received 19 December 1996)

A comprehensive study of different local bonding environments in boron nitride bulk and thin films has been performed by core-level photoabsorption. Several features not present in crystalline reference samples are found in the absorption spectra of the thin films. These are identified as nitrogen vacancies in the hexagonal bonding of BN, nitrogen interstitials, boron clustering, sp^3-like metastable phases, and sp^3 phases. Quantitative information on the concentration and distribution of point defects is easily extracted from the photoabsorption data and is discussed with regard to the formation of additional phases, the B:N ratio in the films, and compared with a random model of defect formation. Information on the stability of the bonding environments is gained by annealing the thin films. Modification of the orientation of the sp^2 hexagonal planes is attained by ion bombardment and annealing, and is monitored by angle-resolved photoabsorption.
[S0163-1829(97)01618-4]

I. INTRODUCTION

Boron nitride is an interesting material for technological applications and for fundamental solid-state physics investigations. It is a compound isoelectronic with carbon and, like carbon can possess sp^2- and sp^3-bonded phases resembling graphite and diamond. BN crystallizes in the sp^2-bonded hexagonal (h-BN), rhombohedral (r-BN), and turbostratic phases, and in the sp^3-bonded cubic (c-BN) and wurtzite (w-BN) phases.[1] As in the case of carbon, fullerene cage and nanotube BN structures have been predicted theoretically,[2] and actually synthesized and characterized.[3,4] A different family of materials is obtained when replacing C-C pairs in graphite with isoelectronic B-N pairs, resulting in C_2BN compounds.[5,6] Regarding other boron compounds, BN is exceptional in the sense that it has standard two-center bonds with conventional coordination numbers, while other boron compounds (e.g., B_4C) are based on the boron icosahedron unit with three-center bonds and high coordination numbers.[7,8]

From an applied standpoint, there is a strong interest in growing BN thin films due to the desirable properties of the material. Hexagonal BN is a good insulator commonly used in vacuum technology, which has also been tried in the thin-film form for microelectronic devices.[9] It is a very inert, refractory material and hence it is commonly used for crucibles in vacuum evaporation techniques. Because of the weak interlayer bonding, h-BN is a soft material which can be used as a lubricant. Cubic BN also has interesting physical properties, very different from the hexagonal phase. It is, after diamond, the second hardest material known, with the advantage over the former that it does not react with ferrous materials making it a preferred hard coating for many industrial applications. Electrically, it is a wide gap semiconductor which can be doped with acceptors and donors more easily than diamond, attracting interest for high-temperature fast microelectronic devices and in visible and ultraviolet optoelectronics. Like diamond, it is also a very good thermal conductor.

The existence of several allotropic forms and fullerene like structures for BN suggests a rich variety of local bonding and poses the questions of how this affects the local electronic structure and how the material accommodates the stress induced in the transition regions between different phases. One would expect point defects to play a crucial role in stress accommodation, but these must also have a strong influence in the electronic structure, since the B—N bond is polar and a point defect will thus be a charged structure. The study of point defects in relationship to the electronic structure is of fundamental interest in these materials. It has been studied theoretically for both h-BN,[10,11] and c-BN,[12] and has attracted experimental spectroscopic work on the variety of color centers that are formed. Techniques sensitive to the sharp electronic levels of the trapped electrons like cathodoluminescence,[13] thermoluminescence,[14] and electron paramagnetic resonance[15,16] have been most widely used. Positron annihilation, a technique commonly used to study vacancies has not shown to be very informative.[17] The draw-

 © 1997 The American Physical Society

back of these techniques is the difficulty in performing a quantitative analysis. Recently, we have shown that near-edge x-ray-absorption fine structure (NEXAFS) is sensitive to point defects in h-BN, and to the formation of metastable phases even in amorphous materials.[18] This is significant since other phase identification techniques like vibrational spectroscopies or x-ray diffraction yield ambiguous results for nanocrystalline[19] and amorphous samples.[20] Serendipitously, NEXAFS also combines chemical selectivity with point-defect sensitivity. In this work we will further demonstrate the use of NEXAFS to study point defects, a field relatively unexplored with this technique.

Point defects in BN are also important with regard to the growth of c-BN thin films. Bulk cubic phase samples are attained by simultaneous annealing and application of high pressures (typically $T\sim 2000$ K, $P\sim 5$ GPa),[21] but can be grown in thin-film form by using deposition techniques assisted by ion bombardment, i.e., with a beam of ions striking the substrate while atomic boron or molecular boron nitride is evaporated. This includes growth methods like plasma-enhanced chemical vapor deposition,[22] radio-frequency sputtering,[23] ion-assisted pulsed-laser deposition,[24] ion-assisted boron evaporation,[25] and simultaneous nitrogen and boron ion bombardment.[26] There is a narrow window of experimental conditions that lead to c-BN formation,[27–29] and previous work has suggested a mechanism mediated by defect formation because the amount of the cubic phase obtained depends on the square root of the ion energy and mass—when different mixtures of N_2 and noble gases are used—whereas a simple momentum transfer mechanism would yield a linear dependence.[30] With regard to the type of defects that are expected, some simulations have been performed indicating a high concentration of vacancies in the surface layers followed by a large number of interstitials in the subsurface region.[31] Some models explain the formation of the cubic phase by the buildup of a biaxial compressive stress,[25] which some authors relate to interstitial Ar or N atoms introduced in the BN matrix during the ion-assisted growth method.[32]

In this work we take advantage of the local sensitivity of the core-level photoabsorption technique to identify the presence of both nitrogen vacancies and interstitials in connection to c-BN growth, and to address some questions concerning the bonding structure of boron nitride in intermediate situations between ordered hexagonal and cubic phases. These metastable and defective phases are attained by ion sputtering, ion bombardment, and annealing treatments of hexagonal BN thin films. We will demonstrate the capabilities of NEXAFS to characterize point defects following a simple quantitative analysis, and illustrate the possibility to obtain orientational information by angle-resolved NEXAFS.

II. EXPERIMENT

To study a range of compositions and bonding modifications as wide as possible, we have measured the B $(1s)$ and N $(1s)$ photoabsorption from a variety of bulk samples and thin films which are briefly described as follows. Reference h-BN samples and c-BN were prepared by attaching crystalline hexagonal and cubic BN powders to a Ta substrate with conductive epoxy. The influence of ion bombarding on the bonding was obtained by sputtering the h-BN crystalline powder sample with Ar^+ ions at 2 keV, a dose of 2×10^{17} cm^{-2} and a current density of 2 μA cm^{-2}. Elemental boron references were obtained from a thin film grown by radio frequency (RF) sputter deposition of a pure boron target using unbalanced planar magnetrons and pure Ar,[18] and from crystalline boron powder epoxied to a Ta sheet. One set of BN thin films was grown on different Si and Ni substrates by magnetron sputtering using a boron target and a mixture of Ar and N_2 gases with different nitrogen compositions ranging from 0 to 55%. Different samples were obtained by applying negative bias voltages from 0 to 400 V (both constant and radio frequency) to the substrate. The RF bias was applied by drawing off approximately 5% of the RF power to the target. Another set of BN thin films was grown on Si substrates by pulsed-laser deposition (PLD) from a hexagonal BN target. For a number of samples, the PLD process was assisted with simultaneous ion bombarding using mixtures of N_2^+ and Ar^+ at energies between 500 and 1000 V. Also, several PLD samples were modified by postdeposition ion implantation with either N_2^+ or Ne^+ at energies between 90 and 180 keV, fluences between 1×10^{17} cm^{-2} and 4×10^{17} cm^{-2} and current densities between 10 μA cm^{-2} and 70 μA cm^{-2}. To further modify the bonding environments, some samples were annealed under vacuum at successively increasing temperatures from room temperature to 1500 K. The BN thin films were annealed by direct current flowing through the Si substrate, the temperature being monitored with an infrared pyrometer calibrated to the emissivity of the Si substrate. Details on each sample preparation will be further discussed in connection with the NEXAFS spectra.

The core-level photoabsorption experiments were conducted at beamline 8.2 of the Stanford Synchrotron Radiation Laboratory[33] and at beamline 8.0 of the Advanced Light Source (LBNL), both of them equipped with spherical grating monochromators. The measurements were performed in the total electron yield mode by recording the photocurrent from the sample with a current amplifier and a multimeter. Simultaneously, the total electron yield was recorded from a metal grid covered with gold that is located upstream from the sample in the x-ray beam path. The signal coming from the sample was normalized by the grid signal to eliminate variations in the x-ray flux. A second normalization was performed to account for absorption from the materials in the beamline optics, by recording the electron yield from a clean Si wafer, i.e., a material whose absorption spectrum should show no structure in the boron and nitrogen regions. This second normalization is not very important for the BN system studied here, but is critical when studying carbon compounds.

Core-level photoabsorption in the electron total yield mode is a technique with an intermediate depth sensitivity, with an electron escape depth of about 50 Å compared with the 5–20 Å of photoemission.[34] This relative bulk sensitivity permits the study of samples grown in other vacuum chambers and transported in air to the analysis chamber. To avoid surface contamination as much as possible, all samples were outgassed at about 500 K in vacuum. Comparison between the spectra before and after outgassing in test samples shows a substantial decrease in the oxygen content (i.e., from ad-

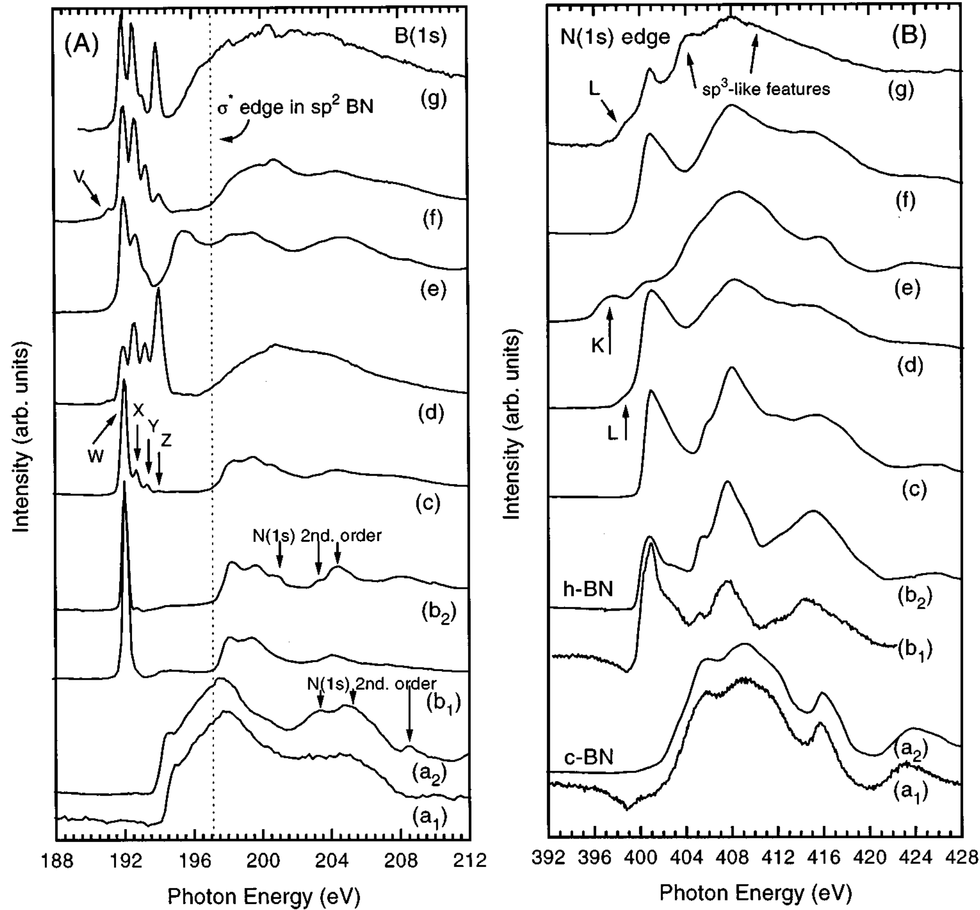

FIG. 1. B ($1s$) and N ($1s$) photoabsorption spectra corresponding to a variety of local environments in the boron nitride system. The same letter in panels (A) and (B) corresponds to the same sample. Curves (a_1) and (a_2) represent a crystalline c-BN reference measured with filtered light to avoid higher orders of diffraction from the monochromator and with unfiltered light, respectively. Curves (b_1) and (b_2) represent a crystalline h-BN reference measured with filtered and unfiltered light, respectively. Note the N features in the B region in second order for the unfiltered measurements, conditions under which the rest of the samples were measured. Curves (c) represent a h-BN thin film grown by pulsed laser deposition exhibiting W-Z peaks in the π^* region, (d) a Ne^+ implanted h-BN thin film, (e) a film RF sputter deposited in an Ar/N_2 mixture from a boron target with an RF bias applied to the substrate to form sp^3 BN, (f) a N_2^+ implanted thin film, and (g) a N_2^+ implanted thin film containing a metastable phase.

sorbed water and carbon oxides) with no changes in the shape of the boron and nitrogen edges.

III. RESULTS AND DISCUSSION

A. General results

Figure 1 shows a series of B ($1s$) and N ($1s$) absorption spectra corresponding to a variety of local environments found in the boron nitride system. This figure illustrates the different features observed in the photoabsorption spectra, a more detailed discussion being given in the following sections. The boron and nitrogen NEXAFS spectra labeled with the same letter correspond to the same sample. In general, the boron edge shows more dramatic differences than the nitrogen edge and therefore we will describe first all the boron spectra. Curves (a_1,a_2) and (b_1,b_2) are reference spectra from crystalline powders of c-BN and h-BN, respectively, the most stable phases with sp^2 and sp^3 bonding. Throughout this work, the c-BN and h-BN standards will be used to compare against the unknown films to determine their bonding. Curves a_1 and b_1 were measured with higher-order light suppression on the diffraction grating. This can be done either by using a carbon filter which absorbs photons with energy over 285 eV or by using synchrotron light from an undulator. Since most of the NEXAFS spectra contained in this paper were measured with unfiltered light, it is important to check how this affects the spectral line shape. Curves a_2 and b_2 correspond to the same samples as a_1,b_1 measured with higher-order light present. The nitrogen absorption edges look identical, but one has to be aware that the boron edges a_2,b_2 contain the nitrogen features in second order as indicated in the figure. We have taken advantage of the second-order signal to calibrate the energy position of the boron and the nitrogen π^* features in h-BN obtaining values of 192.0±0.1 eV and 400.9±0.1 eV, respectively at the peak. Previous work show a scatter in the energy positions of the boron exciton, labeled W in Fig. 1, from 189.5 (Ref. 28) to 193.[35] The photon energy difference between the nitrogen and boron edges was determined to be 208.93±0.02 eV by measuring a Si core level by photoemission at the photon

energies of the boron and the nitrogen π^* features. The absolute energy values of these peaks were then obtained by matching the nitrogen NEXAFS features measured in first and second order.

The boron absorption edge in the c-BN spectrum (curves a_1, a_2) appears at 194 eV and corresponds to transitions from the B (1s) core level to the σ^* states in the conduction band. The NEXAFS spectrum shows a sharp peak—with its maximum at 194.5 eV—near the absorption edge, followed by a broad absorption maximum at 198 eV. The peak at 194.5 eV is probably due to an excitonic state, as is the case in isoelectronic, and similarly bonded, diamond.[36] Some authors have observed an exciton in c-BN as a separate peak at 191.0 eV.[37] However, we do not observe such a feature and by comparing our data with their spectra we find that their energy scale is shifted by about 1 eV to the low-energy side. By correcting their energy scale, the peak they assign to a c-BN exciton would be located at 192.0 eV, hence corresponding to the π^* peak of h-BN phases that may be present in their samples.

The h-BN spectrum (curves b_1, b_2) contains a sharp peak at 192.0 eV corresponding to the B 1s-π^* transition (the π^* resonance offers a clear fingerprint of sp^2 hybridization) in addition to the σ^* absorption edge which now appears at 197.2 eV. NEXAFS references for the other allotropic forms of boron nitride have been published previously,[1] showing that there is almost no difference between the spectra of the hexagonal and rhombohedral sp^2-bonding phases, whereas the differences between spectra measured from cubic and wurtzite sp^3 phases are more pronounced. Those differences are: the boron σ^* edge is located at 195.0 eV in w-BN compared to 194.0 eV in c-BN, there is no excitonic peak at the onset in the wurzite phase, and the maximum of the absorption occurs at 196 eV in a narrower peak than the maximum of the cubic phase located at 198 eV. In any case, it is clear that the σ^* states at energies below 197 eV are related to sp^3 hybridization.

Curve (c) is representative of a BN thin film ($\sim$100 nm thick) grown on a Si(100) substrate by pulsed-laser deposition without nitrogen bombardment. Similar results are obtained for BN grown on Si(111). Also, a similar spectrum is obtained for thin films grown by sputtering in an Ar/N_2 atmosphere if no RF bias is applied to the substrate. It is clear that without nitrogen bombardment only hexagonal-like BN is formed and that the crystal face of the Si substrate has no influence, at least for relatively thick films. The additional features in the π^* region labeled X-Z correspond to N-void defects in the hexagonal bonding, as we have shown previously.[18] In the thin films, one finds four different local environments of boron atoms, since these may be bonded to three nitrogen atoms, two nitrogens, one nitrogen and no nitrogen, and they show up in the NEXAFS spectra as features W-Z, respectively.

A larger intensity ratio of the defect features (X-Z) compared to the stoichiometric BN (W) is observed when either the thin films or the bulk hexagonal BN powders are ion bombarded.[18] Curve (d) shows one such case, corresponding to a h-BN thin film bombarded with Ne^+ ions of 90 keV energy, at a fluence of 4×10^{17} cm^{-2} and an ion current of 40 μA cm^{-2}. Similar results are obtained for Ar^+ bombardment.

When nitrogen ions are used either for the ion-assisted growth process or for postdeposition ion implantation, several modifications of the bonding structure may occur depending on the ion energy, current and fluence parameters, and on performing the bombardment during deposition or after deposition. Generally, postdeposition nitrogen ion bombardment merely creates defects in the hexagonal bonding. Nitrogen bombardment simultaneous with the BN film growth, however, usually results in cubic BN formation, as described in the introduction. Curve (e) corresponds to a BN thin film grown by RF sputter deposition of a pure boron target in a chamber at a base pressure of 5×10^{-6} Pa, with a gas mixture of Ar and N_2 at a pressure of 1.1 Pa with 20–25% N_2 controlled by mass flow, applying an RF bias of -300 V to the substrate to subject the film surface to a constant negative potential, and heating the substrate to 700 K during the deposition. The application of the -300 V RF bias to the substrate causes bombardment with energetic ions during the BN growth and results in formation of sp^3-bonded BN. This film contains about 20% sp^2 and 80% sp^3 phases. Similar results are obtained for thin films grown by nitrogen ion-assisted PLD, another growth method involving energetic nitrogen ions. An important observation is that growth of the sp^3 phase in thin films is always accompanied by the production of defects in the hexagonal bonding, owing to the need for bombardment with energetic ions. Direct comparison with the c-BN reference and the w-BN spectra of Ref. 1 suggests that wurtzite is the sp^3 phase being formed. This point will be discussed in further detail below.

Regarding the bonding modifications induced by postdeposition ion implantation, a new bonding species is found under high ion current bombardment: a fifth boron π^* peak, labeled V, appears at a photon energy lower than that of bulk BN, as shown in curve (f). This spectrum was measured in a h-BN PLD grown thin film, postdeposition implanted with nitrogen ions of 90 keV energy, fluence of 4×10^{17} cm^{-2} and ion current of 60 μA cm^{-2}. The presence of peak V has been repeatedly seen for ion implantation with nitrogen ion currents greater than 20 μA cm^{-2}, although it has never been observed as a very intense feature. Following the same argument used to identify peaks $X-Z$, one can attribute this peak V to boron atoms bonded to four nitrogens. The high coordination number of boron in this case is not surprising, since boron is known to form electron deficient compounds with three center bonds and coordination numbers as high as 6 in elemental boron and other compounds.[7,8] Further justifications for our assignment will be presented in the next section.

Another change in the local structure found after ion implantation is shown in curve (g), corresponding to a PLD grown BN/Si(100) thin film after implantation with N_2^+ at 180 keV at an ion current density of 10 μA cm^{-2}. The most significant change occurs in the σ^* region where a shift in the absorption edge takes place from the sp^2 position at 197.2 to 195 eV, i.e., close to the edge of the reference cubic sample, suggesting the formation of an sp^3-like phase. In fact, 195.0 is the reported value for the σ^* edge in the sp^3 wurtzite phase, further supporting the formation of wurtzite-like BN. However, as it will be shown below in this work, this phase obtained by ion implantation is not stable upon annealing, and it will be referred throughout the paper as a

metastable phase. The features in the π^* region reveal the defect damage induced in the hexagonal phase by ion bombardment.

With regards to the nitrogen edges shown in Fig. 1(B), the features closer to the edge in the c-BN reference curve (a) are a series of broad peaks located at about 406, 409, and 411 eV defining a rather smooth σ^* edge at 402 eV, whereas the h-BN spectrum (b) has a distinct sharp resonance at 400.9 eV which is related to the π^* states. In addition, h-BN has a major feature at about 408 eV and other partially resolved minor peaks at about 403, 406, and 410 eV. Comparison with the nitrogen edges shown in Ref. 1 for the other allotropic forms reveals only very subtle changes between the different sp^2 and sp^3 bonding phases. The hexagonal thin film (c) shows a spectrum similar to the bulk h-BN reference except for a broadening in all the features. The coalescence of the peaks at 401 and 403 eV gives the π^* states a broad triangular shape. The same peak shape is observed in curve (d) for a PLD grown h-BN sample after Ne^+ bombardment, although the features are slightly broader, resulting in the filling of the valleys at about 405 and 413 eV. No sharp and intense defect features equivalent to those found in the boron edge are observed, except for a small shoulder at the absorption onset, labeled L, and located at 399.4 eV. Curve (e), representing the thin film grown by RF sputtering, shows a mixture of the c-BN and h-BN features plus a new peak, labeled K, at 397.9 eV. Curve (f), corresponding to the high current N_2^+ bombardment yielding the fifth boron π^* peak in Fig. 1(A) shows up as a normal h-BN thin film, with a small intensity of peak L. Curve (g) is composed of sp^2 and sp^3-like features (the latter marked with arrows) in addition to peak L.

A number of questions such as the origin of peaks K and L in the nitrogen edge and their relationship to peaks V–Z in the boron edge, the relationship between defect peaks and stoichiometry, or the conditions to obtain different phases, arise at this point. They are discussed in detail in the forthcoming sections.

B. New features on the boron 1s π^* edge: Nitrogen vacancies

The photoabsorption B (1s) π^* peaks of multiple BN samples with different defect ratios have been analyzed—their peak position, width, and intensity ratio being determined by curve fitting the spectra with Gaussian curves. Some of these fits, corresponding to a broad range of vacancy ratios, are shown in Fig. 2. The vacancy ratio is derived from the relative intensities of peaks W–Z. According to the local environments corresponding to peaks W–Z, the number of vacancies per boron atom is 1/3 for a boron atom contributing to peak X, 2/3 of a vacancy for atoms of type Y, and 1 vacancy for atoms of type Z. Therefore, the experimental vacancy ratio (v) is determined by the equation $v=(0.33X+0.66Y+Z)/(W+X+Y+Z)$, being $W-Z$ the intensities of the corresponding peaks.

Regarding the energy and line shape of the B (1s) defect peaks it is clear that the peak positions are independent of the relative heights for peaks $W-Z$. Therefore the energy shift only depends on the number of nitrogen nearest neighbors. For all cases, the separation between peaks $W-X$ and $X-Y$ is 0.63 ± 0.03 eV and the line shape is the same for all

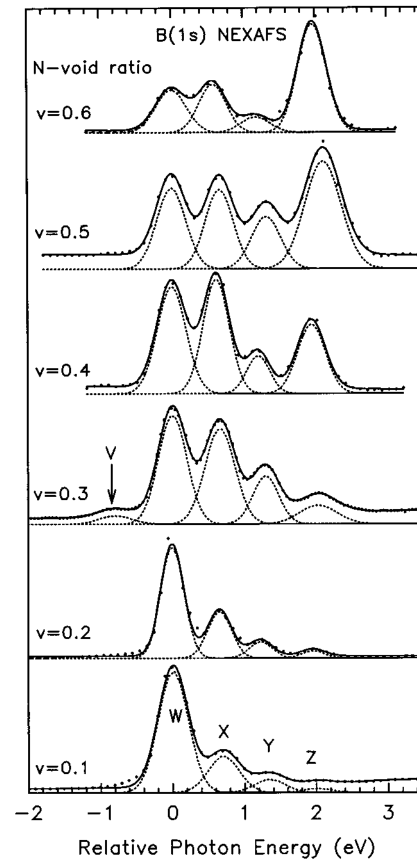

FIG. 2. B (1s) π^* peaks from selected samples containing a nitrogen vacancy fraction between 0.1 and 0.6, curve fitted with four Gaussians.

three with a full width at half maximum (FWHM) of 0.45 eV. However peak Z is somewhat different. Depending on the sample its width can be the same as peaks $W-Y$ or it can be slightly wider (up to 0.60 eV). We have found no direct relationship between the width and either the relative intensity of peak Z or the details on the thin-film growth method. Also the peak separation between peaks $Y-Z$ is different from $W-X$ and $X-Y$, ranging from 0.75 to 0.80 eV. A possible scenario explaining the different behavior of peak Z follows. The defects corresponding to peaks $X-Y$ are consistent with the hexagonal network of B-N atoms. However, for the case of peak Z, a boron atom surrounded by three vacancies is not a stable situation, the formation of B—B bonds being more likely. These B—B bonds can be formed within the hexagonal framework by the location of a boron atom in a nitrogen site or by the bonding of boron in a hexagonal site to boron in an interstitial site, or out of the hexagonal framework by formation of boron clusters, probably the boron icosaedra found in most boron-rich compounds. These different possibilities explain the differences of peak Z in energy position and width compared to peaks X and Y.

Peak V on the left side of the main peak appears in some of the samples, its width being similar to that of peaks W–Y but with an energy shift V–W of 0.78 eV. A different energy shift compared to the W–X or X–Y is not surprising since the bonding of a boron atom to four nitrogens is not possible within the hexagonal framework. A significant

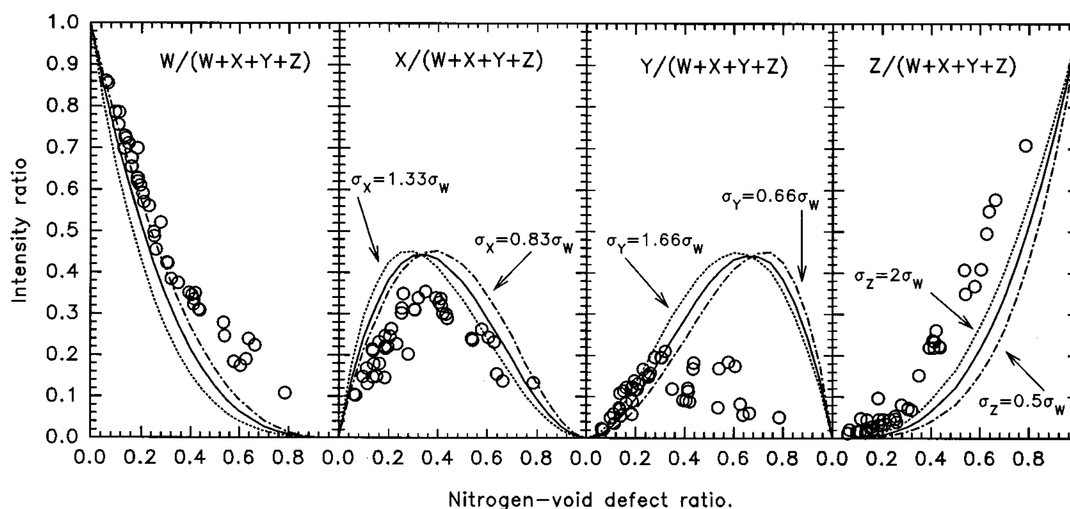

FIG. 3. Dots: experimental intensity ratios for the π^* peaks of a series of BN films as a function of the nitrogen vacancy percentage. Solid lines: fraction of boron atoms surrounded by 0, 1, 2, and 3 vacancies in a random model of nitrogen vacancies. Dotted and solid-dotted lines: same as the solid lines corrected for an hypothetical change of the cross section with the number of nitrogen nearest neighbors.

change in bond character must exist, either in strength, length, or nonplanarity of the BN_4 moiety, while still retaining sp^2-like character.

An important question is raised by the relative intensity of peaks $W-Z$: whether they just follow a random distribution of vacancies or if thermodynamics makes some defect configurations more stable than others. To test this, we have performed a simple calculation on a hexagonal BN cluster consisting of 10^6 atoms in a single hexagonal plane and removing randomly nitrogen atoms until a certain proportion of N-void defects is created. Nitrogen vacancy ratios ranging from 0, i.e., a perfect BN crystal, to 1, i.e., total depletion of nitrogen, were considered. For each value of the nitrogen vacancy ratio, the number of boron atoms surrounded by single, double, and triple nitrogen voids were tabulated along with B that remains bonded to three nitrogen atoms. Figure 3 shows the intensity ratios found experimentally (dots) and those corresponding to the random distribution of vacancies (lines), plotted as a function of the vacancy ratio.

The solid lines shown for each panel of Fig. 3 represent the fraction of boron atoms surrounded by 0, 1, 2, and 3 nitrogen vacancies. They are obtained numerically by the method described above and do not correspond to a fit to any analytic function. The experimental data follow to first order the theoretical curves, but some discrepancies are also clear. The overall agreement substantiates our assignment of peaks $X-Z$ to nitrogen-void defects, and that the calculation method of the experimental vacancy ratio is correct. Note that the random model does not take into account any kinetics or consideration of stability, but is simply a metric (albeit a useful one) for interpreting the progression and fluctuation of defect concentration in these metastable thin films. Note also that we have intentionally avoided calling these nitrogen-void defects ''nitrogen vacancies,'' because we cannot assure that the nitrogen vacant sites are not occupied by other chemical species (e.g., hydrogen) hence resulting in substitutional defects, even if they can be considered as vacancies from the nitrogen standpoint.

Another question is how a different absorption cross section would affect the theoretical curves. The solid curve displayed in each panel in Fig. 3 corresponds to the assumption of a single value for the cross section for all peaks. To check this point we have also assumed a linear variation of the cross section from peak W to Z. The dotted curve corresponds to a cross section for peak Z twice that of peak W, and the dot-and-dash curve corresponds to a cross section for peak Z half that of W. Peaks X and Y are given intermediate values of the cross section in a linear relationship. The displayed curves illustrate that the changes introduced by the different cross sections are rather small and that they cannot explain the discrepancies between the model and the experiment. Moreover, different values of the cross section exhibit opposite trends in the development of the model curves for peaks W and Z: if the intensities are higher than the single cross section model in one case, it is lower in the other case and vice versa. The experiment shows, however, that for both W and Z the intensities are higher than the single cross section model predicts. Therefore, the discrepancies are due to the different thermodynamic stability of different defect configurations, and suggest that a B-N_3 (peak W) and a B-B_3 configuration (peak Z) are the most stable. This is intuitively true but should be interrogated rigorously with theory. A single vacancy adjacent to a boron atom (peak X) is a rather stable defect, since the discrepancy between experiment and model is small, and equally stable along the whole vacancy ratio range. However, two vacancies adjacent to a boron atom (peak Y) is only stable for a vacancy fraction lower than 1/3. Over this value this configuration is very unstable, encouraging the formation of B—B bonds.

One can create many combinations of defects and compare them with Fig. 3 to check their stability. Some of these are pictured in Fig. 4. Panel (a) represents a simple mechanism to explain the decrease of boron atoms of type X. This is the coalescence of three single vacancy defects, i.e., nine type X atoms, to form a triple vacancy of type Z and six type X defects. One can write this as the following reaction in-

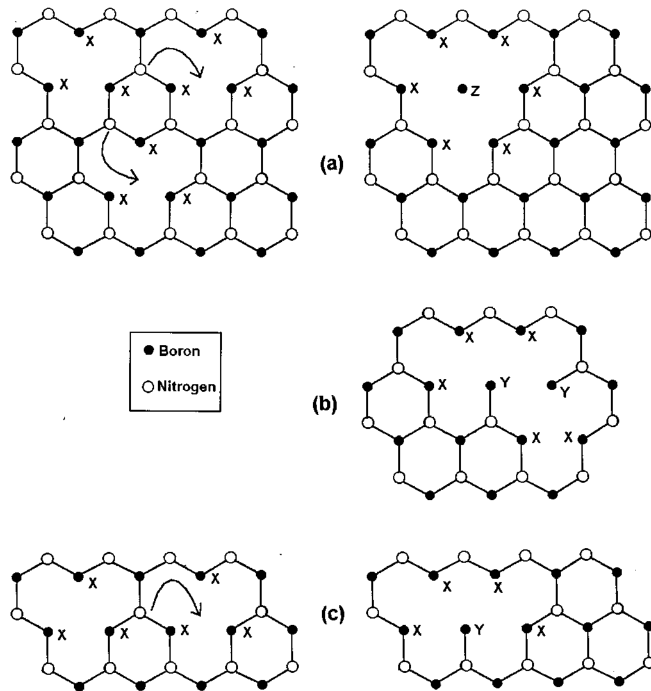

FIG. 4. Different combinations of nitrogen vacancies and plausible atom jumps to more stable configurations according to Fig. 3.

volving types of boron atoms: $9X \rightarrow 6X + Z + 2W$. This reaction would explain the higher number of type W and Z atoms and the lower number of X atoms found experimentally compared to the model. To take place, at least two vacancy jumps must occur so that the three vacancies get together, as indicated in Fig. 4 by arrows. Another configuration containing three vacancies is displayed in panel (b). We believe that this configuration is rather stable, since it represents a X/Y ratio of 3 which is the one found experimentally for a vacancy ratio lower than 1/3. When the X/Y ratio gets smaller, the high Y density turns unstable, and formation of W and Z environments is preferred. Another configuration containing type Y atoms result from the coalescence of only two of the vacancies yielding type X atoms, and can be written as $6X \rightarrow 4X + Z + W$. This is shown in panel (c) of Fig. 4. To further study the creation and mobility of different defect configurations one would relate the vacancy jump probability and activation energies with the observed distribution of atoms $W-Z$, but it is beyond the scope of this paper. Our simple model is useful for illustrating various defect annihillation mechanisms and relative stabilities.

C. Additional features on the N (1*s*) edge: Interstitial nitrogen

As shown in the previous section, nitrogen vacancies are common defects in ion bombarded *h*-BN. Part of the nitrogen atoms displaced from their crystalline sites move to interstitial positions along with a fraction of the impinging nitrogen ions that can remain embedded in the material. The latter results in a nitrogen enrichment of BN films by nitrogen bombardment that has been previously reported and attributed to interstitial N.[38] We have also seen similar evidence in our films as is shown below. In this section we will discuss the observation of peaks in the N (1*s*) spectra related to the interstitial nitrogen atoms.

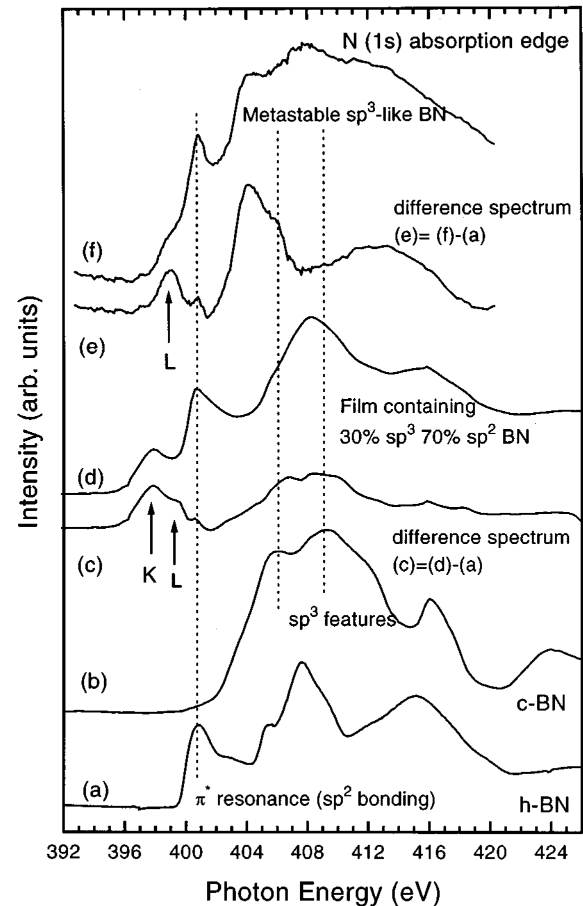

FIG. 5. N (1*s*) photoabsorption spectra illustrating the appearance of features *K*, *L* related to interstitial nitrogen and features related to the metastable phase. Curves (a) and (b) represent reference *h*-BN and *c*-BN samples, respectively. Curve (d) corresponds to a film grown by RF sputtering containing sp^3 and sp^2 bonded BN, the additional features being highlighted in curve (c) by subtracting the *h*-BN reference spectrum. Curve (f) corresponds to an *h*-BN film grown by pulsed-laser deposition, eventually implanted with N_2^+ ions and producing the formation of a metastable phase, the additional features being highlighted in curve (e) by subtracting the *h*-BN reference spectrum.

We have not observed three defect peaks equivalent to those found in the B (1*s*) NEXAFS that support the existence of boron vacancies, but additional features have developed in the sputtered films. The additional features in the nitrogen photoabsorption do not appear generally as clearly resolved peaks. It is therefore useful to subtract the spectrum from an *h*-BN reference to highlight them, as has been done for two films in Fig. 5. Curves (a) and (b) in Fig. 5 correspond to the *h*-BN and *c*-BN references. Curve (d) corresponds to a film grown by RF sputtering containing $\sim$30% sp^3 and 70% sp^2 BN. The sp^3 features are not resolved in the nitrogen spectrum, although they are evident in the corresponding boron spectrum (not shown). However, the presence of sp^3-related features is clear when subtracting the *h*-BN reference, as is illustrated in curve (c). In addition to the cubiclike features, two peaks appear at 397.8 eV, labeled *K*, and at 399 eV, labeled *L*. Curve (f) corresponds to the

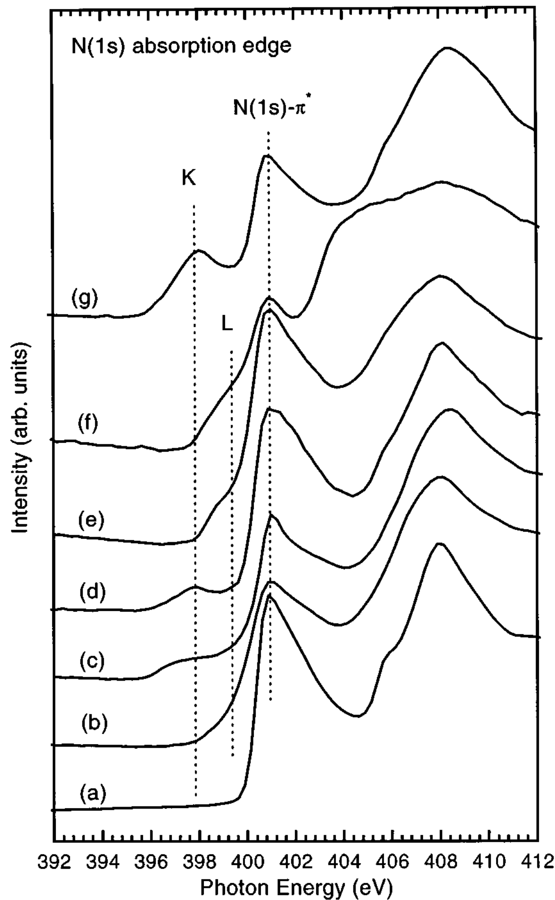

FIG. 6. Low-energy side of N $(1s)$ photoabsorption spectra of a series of thin films, illustrating the appearance of peaks K, L related to interstitials in sp^3 and sp^2-bonded BN, respectively. Curve (a) represents a h-BN film grown by pulsed-laser deposition containing a fraction of 0.05 nitrogen vacancies, (b) a h-BN PLD grown film with a fraction of 0.15 N-void defects, (c) a film grown by RF sputtering with a 0.15 vacancy ratio, (d) a film grown by RF sputtering containing a small amount of sp^3-bonded BN, (e) an h-BN film N_2^+ implanted with a 0.45 vacancy ratio, (f) a N_2^+ implanted film containing the metastable phase, and (g) a RF sputtering grown film containing 30% sp^3-bonded BN.

metastable phase obtained by ion implantation—already presented in Fig. 1 curve (g)—, with additional nitrogen features appearing clearer in the difference spectrum (e) that results from subtraction of the h-BN reference. Two clear peaks at 404 and 406 eV are present that do not line up with either the cubic or the hexagonal features, indicating that nitrogen in a different bonding environment has been formed. Curve (e) also shows the L peak at 399 eV. Once the additional features—peaks $K-L$ and metastable BN phase features—have been clearly identified by reference sample subtraction, we extend the study to a variety of samples to gain some information on their origin.

Figure 6 presents a series of nitrogen edges containing the K and L features in the low-energy side of the spectra. Curve (a) corresponds to a hexagonal thin film grown by PLD containing few defects (the vacancy fraction derived from the boron π^* peaks is 0.05). The nitrogen edge is abrupt and can be nicely fit with a straight line from the onset to a position near the π^* maximum. We have always observed this phe-

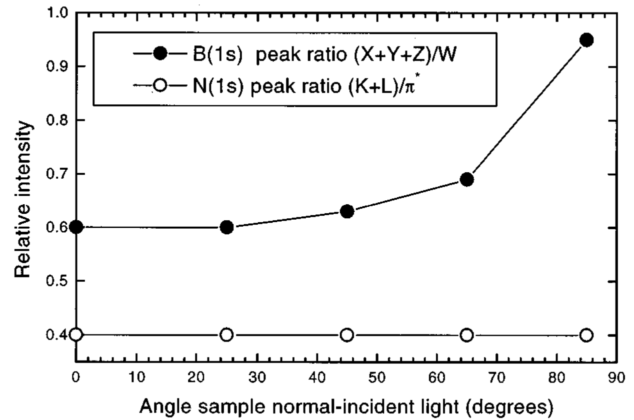

FIG. 7. Intensity ratio of defect over nondefect features for the boron and nitrogen spectra as a function of the angle between the sample normal and the incident light. Grazing incidence results in surface sensitivity measurements indicating the location of nitrogen vacancies at the surface and interstitial nitrogen in the subsurface.

nomenon for films with a nitrogen vacancy ratio lower than 0.1. However, over this value the additional features can be detected. Curve (b) corresponds to a PLD grown thin film with a vacancy fraction of 0.15, showing a shoulder at the onset of the absorption spectra due to an unresolved L peak. Curve (c) represents another PLD film with a similar vacancy ratio, which exhibits shoulders at the positions of both K and L peaks. Curve (d) was measured from a film with a similar vacancy ratio grown by RF sputtering showing a clearly resolved K peak. Curves $(e-g)$ represent different films exhibiting the new features with greater intensity. Curve (e) corresponds to a highly defective h-BN film with a vacancy fraction of 0.45. Curve (f) represents a h-BN film containing the metastable phase and a 0.65 vacancy ratio in the hexagonal bonding, and curve (g) represents a film containing about 70% sp^2-BN and 30% sp^3 BN with a 0.2 vacancy ratio in the sp^2 phase.

An important qualitative result from Fig. 6 is that peak L is always present whenever the vacancy fraction in the hexagonal phase is larger than 0.1, and that the intense peak K is only observed for samples containing a significant proportion of sp^3 BN [see Fig. 1 curve (e) for a thin film containing 80% sp^3-bonded BN]. This suggests that peak L is related to nitrogen atoms in interstitial sites of the hexagonal network, while peak K is related to interstitials in the sp^3-bonded network. We will substantiate this with additional analysis. The defect peaks in the nitrogen edge are not detected for a concentration of defects smaller than 0.1 because they are not located in the near-surface region. This was predicted by TRIM calculations,[31] and can be seen from the angle-resolved NEXAFS results of Fig. 7. In this figure the ratio of defect peaks over nondefect peaks for the boron photoabsorption and for the nitrogen NEXAFS is displayed as a function of the angle between the sample normal and the incident light for the sample represented in Fig. 6 curve (g). The defect ratio for the B $(1s)$ signal is related to the number of vacancies and shows a clear increase when going to glancing incidence, i.e., when increasing the surface sensitivity. However, the defect ratio for the N $(1s)$ signal does not show this surface sensitivity dependence. The same result is obtained for other samples.

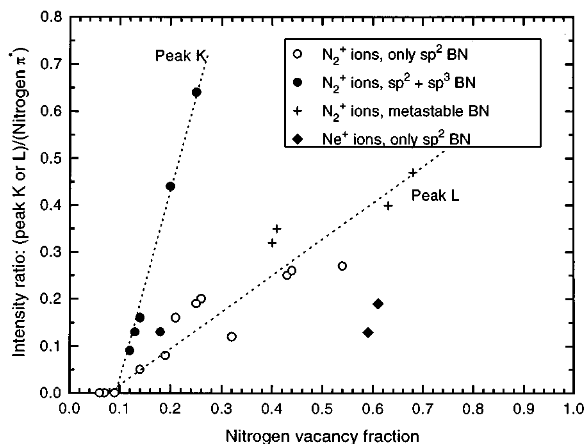

FIG. 8. Intensity ratio of peaks K-L over the N π^* peak vs the nitrogen vacancy ratio indicating the linear relationship between the number of interstitial nitrogen atoms and the number of nitrogen vacancies for different sets of samples.

Quantitative information is derived from Fig. 8, showing that there is a linear relationship between the intensity of the nitrogen peaks $K-L$ and the nitrogen vacancy fraction on the h-BN network, the latter value computed from the boron π^* features $W-Z$. No nitrogen K or L features are detected for a vacancy ratio lower than 0.1. Over this value two distinct paths are observed: development of the nitrogen peak K when sp^3-BN is attained, and development of the nitrogen peak L when defective h-BN or the metastable sp^3-like phase are formed. The Ne^+ sputtered samples show a lower intensity of the nitrogen defect peak compared to the N_2^+ sputtered ones, due to the absence of trapped nitrogen ions that remain embedded in interstitial positions of the BN matrix.

A linear relationship between features $K-L$ and the nitrogen vacancy ratio is expected if all the interstitial nitrogens have their origin in nitrogen vacancies. However, this is not the case here because there is a nitrogen enrichment when nitrogen ions are used. The linear relationship of Fig. 8 therefore indicates that the nitrogen enrichment is still roughly proportional to the number of vacancies because both the number of vacancy-interstitial pairs and the number of ion-trapped interstitials are proportional to the number of ions striking the surface. The larger value of the slope for the development of peak K compared to the development of peak L is explained because the intensity of the peaks K and L is normalized to the intensity of the N $(1s)$ π^* peak in the same spectrum. The films exhibiting peak K have a large fraction of sp^3-bonded BN which does not contribute to the N $(1s)$ π^* peak. When correcting the K/π^* intensity to the content of sp^2 BN on the film, the line representing the development of peak K lines up with the line corresponding to the development of peak L. This indicates that the nitrogen content in the films exhibiting sp^3 phases is roughly the same as that in the h-BN films.

The nature of the metastable phase is unknown, exhibiting on the one hand σ^* features in the B $(1s)$ NEXAFS that resemble an sp^3-bonding configuration, but on the other hand, a trend in the nitrogen L peak resembling sp^2 phases and a series of features in the N $(1s)$ NEXAFS that corre-

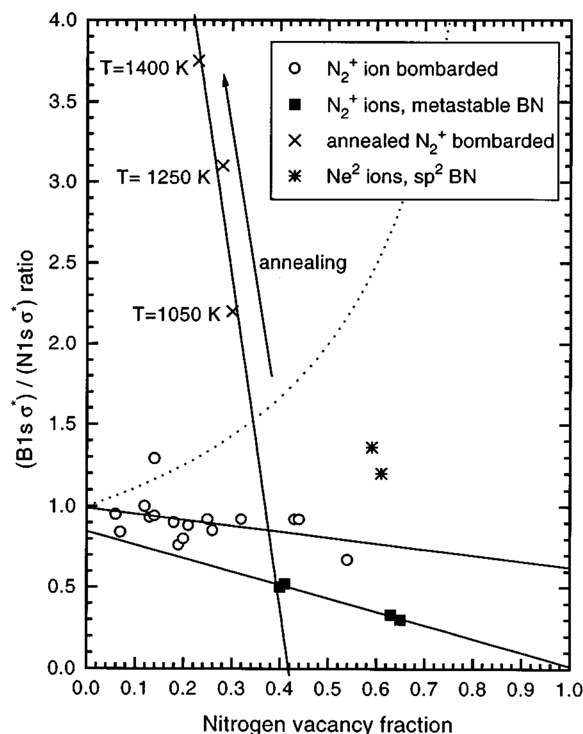

FIG. 9. Intensity ratio of boron over nitrogen measured at the σ^* edges vs the nitrogen vacancy ratio illustrating the nitrogen enrichment for defective samples, the higher nitrogen content of the metastable phase, and the nitrogen outgassing upon annealing.

spond neither to sp^2 nor to sp^3 BN. It can be correlated with mechanical properties of the film,[39] but there is not enough spectroscopic information to conclude the exact nature of the bonding. Two possibilities that might account for the observed behavior are a network of tetrahedrally coordinated boron connected by azide (—N═N—) moieties, or a boron-rich solid resembling B_4C with nitrogen atoms instead of carbon, a bonding configuration that has been previously proposed by other authors to explain Raman and x-ray-diffraction results.[40]

The nitrogen enrichment during nitrogen bombardment is clear from Fig. 9, in which the boron:nitrogen ratio in the films is plotted versus the nitrogen vacancy ratio. Different symbols represent different types of thin films. The dotted curve corresponds to the relationship that would appear if no interstitial nitrogen were present at all. Direct comparison of the experimental points with the hyperbolic curve indicates not only the presence of interstitial nitrogen atoms, but the nitrogen enrichment with N_2^+ bombardment as well. The experimental B:N fraction was computed from the intensity ratio of the maximum of the σ^* features in both the boron and the nitrogen absorption edges. The σ^* features are a better choice than the π^* because the latter depends strongly on the orientation of the π^* orbital with respect to the direction of the electric vector of the incident x-rays beam. We will discuss these angular effects in the next section when studying the orientation of the basal planes in BN. Figure 9 reveals the different behavior for four different sets of samples. (1) The BN films bombarded with N_2^+—including h-BN films, samples containing sp^3-bonded BN, films grown with ion assistance, and films ion implanted after

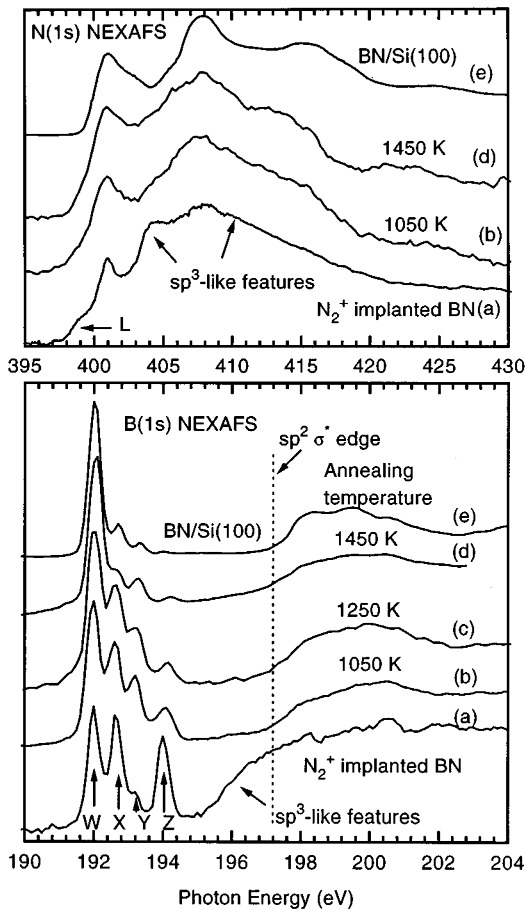

FIG. 10. B $(1s)$ and N $(1s)$ photoabsorption spectra corresponding to the annealing of the metastable phase illustrating the disappearance of the related features at 1050 K, and the eventual decrease of the vacancy-related peaks.

growth—exhibit a B:N ratio close to unity, with a general trend to nitrogen enrichment for larger vacancy ratios. No clear dependence of the nitrogen content with the details of the film preparation is observed. (2) The h-BN films bombarded with noble gases are nitrogen deficient compared to the samples bombarded with nitrogen, providing evidence of the trapping of nitrogen in the BN matrix. (3) The films containing the metastable phase are richer in nitrogen than the h-BN for a similar vacancy ratio. (4) The annealed samples show a dramatic loss of nitrogen, indicating the outgassing of the interstitial nitrogen.

D. Thermal annealing: Order recovery, orientation, stable and unstable phases

We have checked the stability of the sp^3 and the metastable phases by annealing. The most stable phase of boron nitride is the hexagonal one, the transition temperature from cubic to hexagonal being about 1840 K.[41] Since we have limited our study to temperatures of 1500 K, below the melting point of the Si substrate (1700 K), no changes should take place for a stable sp^3-BN phase.

Figure 10 shows a series of boron and nitrogen spectra corresponding to the annealing of the metastable sp^3-like phase. Curves (a) were measured from the sample before heating, showing the sp^3-like features in both the B $(1s)$ and N $(1s)$ NEXAFS. Curves (b) were measured from the sample after annealing to a temperature of 1050 K, showing that the sp^3-like features are no longer present. The boron edge also shows the fading of the defect peaks on the π^* region. Annealing to higher temperatures only results in recovery of hexagonal order as evidenced by the decrease in the intensity of the boron defect peaks of curves (c-d). The spectra (d) of the film annealed to 1450 K are very similar to those of a fresh film grown by PLD without ion bombardment that are displayed as curves (e).

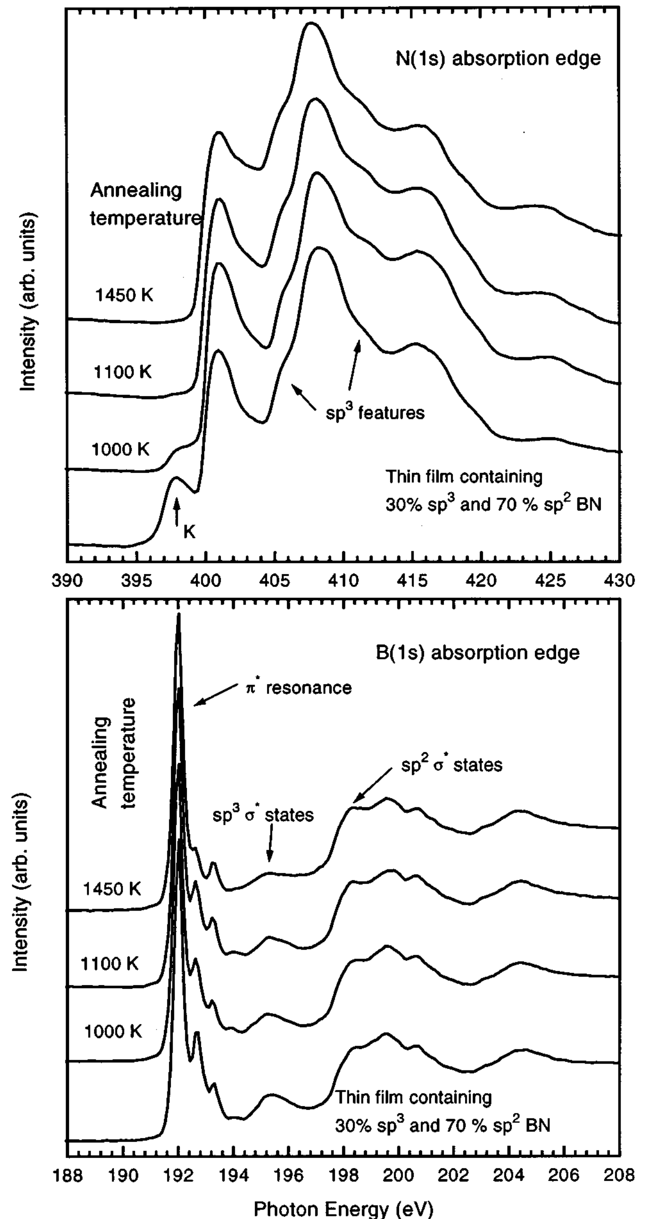

FIG. 11. B $(1s)$ and N $(1s)$ photoabsorption spectra corresponding to the annealing of a film containing 30% sp^3-bonded BN, illustrating the stability of the phase synthesized by RF sputtering, and the outgassing of interstitial nitrogen at ~ 1000 K.

Figure 11 shows a similar series of spectra for the annealing of a thin film grown by RF sputtering containing $\sim 30\%$ sp^3-BN and 70% sp^2-BN. Curves (a) are from the sample before annealing. Curves (b) were measured after

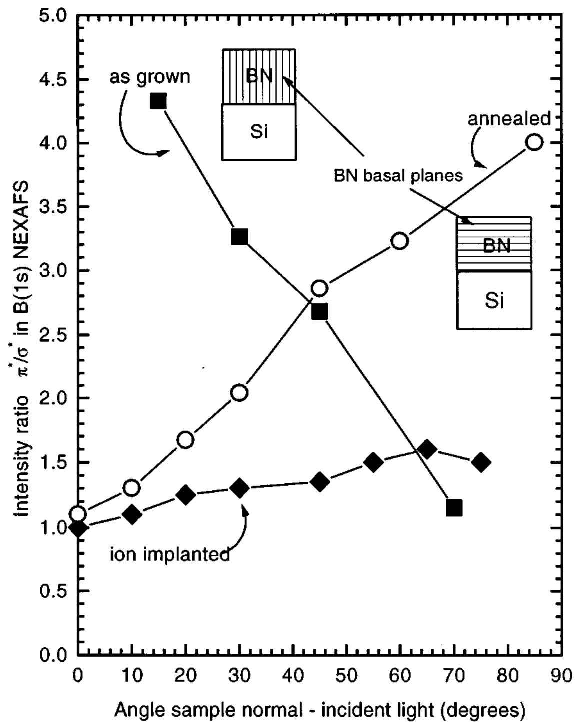

FIG. 12. Ratio of the intensity from the B $(1s)$ photoabsorption features π^*/σ^* vs the angle between the sample normal and the incident light for a h-BN thin film as grown, after ion implantation and after annealing, illustrating the change in the orientation of the basal planes.

annealing to 1000 K. No changes in the boron spectrum occur regarding the sp^3-sp^2 ratio indicating the stability of the first phase. However the extra peak K in the nitrogen spectrum has decreased significantly, showing that peak K is not due to the sp^3 bonding, although it always appears in connection to its growth in thin-film form as discussed in the preceding section. Peak K originates from nitrogen atoms in interstitial positions of sp^3 BN, and annealing over 1000 K results in outgassing of these N interstitials. Peak K is no longer present after annealing to 1100 K, as shown in curves (c), although the sp^3 features remain. Annealing to higher temperatures has no additional effect on the nitrogen and boron spectra, apart from the successive decrease of the defect peaks in the B $(1s)$ π^* region, confirming the stability of the sp^3 phases grown by the RF sputtering.

An interesting result concerns the orientation of the hexagonal planes in boron nitride. Angle-dependent measurements of the NEXAFS signal were performed, taking advantage of the linearly polarized nature of synchrotron radiation. The selection rules yield a cosine-squared dependence on the angle between the π^* bond and the electric-field vector, with the maximum for the basal planes parallel to the incident light and a zero intensity when they are perpendicular.[42] Figure 12 displays the ratio between the height of the peak W in the B $(1s)$ π^* region and the maximum of the σ^* intensity for the as-grown thin film, the film after ion implantation considered in Fig. 10, and the same thin film after annealing. The reversal in the orientation of the basal planes is clear from this figure. For the as-grown samples, the hexagonal planes are oriented perpendicular to the surface, as it has been determined previously for the ion-assisted PLD samples by electron diffraction,[25] NEXAFS,[43] and electron microscopy.[44] The ion-implanted samples do not show any significant anisotropy in the π^*/σ^* ratio, indicating a random orientation of the fragments of basal planes. When the sample is annealed, the basal planes orient again but, in spite of the initial situation, they are now parallel to the surface, at least in the surface region where NEXAFS is sensitive.

A final result refers to the influence of the ion bombardment parameters on defect formation and how self-annealing affects this. In principle, one expects a higher concentration of defects when a larger ion current density or more energetic ions strike the surface. However, we have found that for ion implantation at room temperature the nitrogen vacancy fraction near the surface is larger for nitrogen ions of 90 keV than for ions of 180 keV, at a constant value of current density of 20 μA cm^{-2} and total dose of 2×10^{17} cm^{-3}, and that the number of defects is also larger for an ion current of 20 μA cm^{-2} than for ion currents of 40 and 60 μA cm^{-2} at a constant dose of 2×10^{17} cm^{-3} and ion energy of 180 keV. The explanation for this is a self-annealing effect due to local heating by the ions when the ion bombardment conditions are very energetic. Indeed, we have found that the films presumably self-annealed, i.e., those containing less defects than others bombarded with less severe conditions, show a certain orientation of the basal planes parallel to the surface, although not as clear as in the film presented in Fig. 12.

IV. CONCLUSIONS

We have performed a detailed study of point defects in boron nitride by NEXAFS spectroscopy in connection to the appearance of bonding phases during thin-film growth. The sensitivity of NEXAFS to these defects can be used to better understand the chemistry and morphological changes that occur during the metastable growth conditions of thin films. This is particularly interesting for complex systems like nitrides, carbides, and borides which are well suited to photoabsorption studies and are very technologically attractive materials in thin-film form. This is even more important when the thin films lack long-range order, and techniques like x-ray diffraction or vibrational spectroscopies yield ambiguous results in the phase characterization.

Regarding the boron-nitride system studied here, we have identified the signature in the photoabsorption spectra of nitrogen vacancies and interstitial nitrogen. No features related to the presence of boron vacancies have been observed. Information on the stability of different arrangements of nitrogen vacancies can be gained by direct comparison with a simple model based on the random distribution of nitrogen voids. Interstitial nitrogen appears as two distinct features depending on them being embedded in a hexagonal or a cubiclike network.

There are several implications about thin-film growth conditions and current models of c-BN formation from this work. We have observed that the attainment of sp^3-bonded BN is always accompanied by nitrogen vacancies in the remaining sp^2-bonded material and a significant fraction of interstitial nitrogen embedded in the cubiclike phase. The latter can be easily eliminated by eventual annealing to

~1000 K without additional changes in the film composition. The presence of point defects support the current models that involve defect intermediates in c-BN formation. However, we have not observed any appreciable difference in the nitrogen enrichment between h-BN films containing interstitial nitrogen, and films containing the sp^3 phase. Stable sp^3 phases are only attained with ion-assisted techniques. Ion implantation after the thin-film growth permits us to obtain N-rich films with a similar B:N ratio compared to the ion-assisted growth films, but that does not result in formation of a stable sp^3 phase. Annealing at temperatures over 1000 K outgasses the interstitial nitrogen and also results in a reduction of the nitrogen vacancy fraction. This explains the existence of an optimal temperature for c-BN growth (about 700 K), since over the optimal value the concentration of point defects will decrease by annealing. The same stands for the ion energy and ion current during bombardment, which may produce self-annealing effects by local heating.

Finally, a metastable phase has been detected by the presence of features in both the B (1s) and N (1s) photoabsorption spectra. This phase has been observed when severe ion bombardment is performed and the nitrogen vacancy fraction exceeds a value of 0.4.

ACKNOWLEDGMENTS

We are indebted to R. Hill for his technical support, and the SSRL and ALS staffs for their help. We would like to thank Dr. J. V. Mantese and his group at GM Research Labs for implanting the BN films, and D. Chance for his technical support. This work has been supported by the Division of Materials Sciences, Office of Basic Energy Science, and performed under the auspices of the U.S. Department of Energy by Lawrence Livermore National Laboratory under Contract No. W-7405-ENG-48, and the Advanced Light Source, LBNL under Contract No. DE-AC03-76SF00098. I.J. acknowledges financial support from the Spanish Ministerio de Educación y Ciencia.

---

*Current address: Instituto de Ciencia de Materiales de Madrid (CSIC). Cantoblanco, E-28049, Spain.

[1] L. J. Terminello, A. Chaiken, D. A. Lapiano-Smith, G. L. Doll, and T. Sato, J. Vac. Sci. Technol. A **12**, 2462 (1994).

[2] M. Saunders, Science **253**, 330 (1991).

[3] S. Iijima, Nature (London) **354**, 56 (1991).

[4] A. Loiseau, F. Willaime, N. Demoncy, G. Hug, and H. Pascard, Phys. Rev. Lett. **76**, 4737 (1996), and references therein.

[5] K. Kobayashi and N. Kurita, Phys. Rev. Lett. **70**, 3542 (1993).

[6] M. O. Watanabe, S. Itoh, K. Mizushima, and T. Sasaki, Appl. Phys. Lett. **68**, 2962 (1996).

[7] K. Wade, *Electron Deficient Compounds* (Nelson, London, 1971).

[8] D. Emin, Phys. Today **40** (1), 55 (1987).

[9] T. K. Pauli, P. Bhattacharya, and D. N. Bose, Appl. Phys. Lett. **56**, 2648 (1990).

[10] A. Zunger, J. Chem. Phys. **62**, 1861 (1975).

[11] A. M. Dobrotvorskii and R. A. Evarestov, Phys. Status Solidi **66**, 83 (1974).

[12] V. A. Gubanov, Z. W. Lu, B. M. Klein, and C. Y. Fong, Phys. Rev. B **53**, 4377 (1996).

[13] A. M. Zaitsev, A. A. Melnikov, V. B. Shipilo, and E. M. Shishonok, Phys. Status Solidi **94**, K125 (1986).

[14] A. Katzir, J. T. Suss, A. Zunger, and A. Halperin, Phys. Rev. B **11**, 2370 (1975).

[15] E. Y. Andrei, A. Katzir, and J. T. Suss, Phys. Rev. B **13**, 2831 (1976).

[16] S. Lin, I. M. Brown, and B. J. Feldman, Solid State Commun. **96**, 421 (1995).

[17] H. Murakami and T. Endo, J. Phys. Condens. Matter **1**, SA131 (1989).

[18] I. Jiménez, A. Jankowski, L. J. Terminello, J. A. Carlisle, D. G. J. Sutherland, G. L. Doll, J. V. Mantese, W. M. Tong, D. K. Shuh, and F. J. Himpsel, Appl. Phys. Lett. **68**, 2816 (1996).

[19] R. J. Nemanich, S. A. Solin, and R. M. Martin, Phys. Rev. B **23**, 6348 (1981).

[20] D. M. Gruen, A. R. Krauss, C. D. Zuiker, R. Csencsits, L. J. Terminello, J. A. Carlisle, I. Jiménez, D. G. J. Sutherland, D. K. Shuh, W. M. Tong, and F. J. Himpsel, Appl. Phys. Lett. **68**, 1640 (1996).

[21] O. Mishima, Mater. Sci. Forum **54–55**, 313 (1990).

[22] H. Saitoh and W. A. Yarbrough, Appl. Phys. Lett. **58**, 2482 (1991).

[23] M. Mieno and T. Yoshida, Jpn. J. Appl. Phys. **29**, L1175 (1990).

[24] A. K. Ballal, L. Salamanca-Riba, G. L. Doll, C. A. Taylor II, and R. Clarke, J. Mater. Res. **7**, 1618 (1992).

[25] D. R. McKenzie, D. J. H. Cockayne, D. A. Muller, M. Murakawa, S. Miyake, S. Watanabe, and P. Fallon, J. Appl. Phys. **70**, 3007 (1991).

[26] H. Hofsass, C. Ronning, U. Griesmeier, M. Gross, S. Reinke, and M. Kuhr, Appl. Phys. Lett. **67**, 46 (1995).

[27] D. J. Kesker and R. Messier, J. Appl. Phys. **72**, 504 (1992).

[28] T. A. Friedmann, P. B. Mirkarimi, D. L. Medlin, K. F. McCarty, E. J. Klaus, D. R. Boehme, H. A. Johnsen, M. J. Mills, D. K. Ottensen, and J. C. Barbour, J. Appl. Phys. **76**, 3088 (1994).

[29] D. L. Medlin, T. A. Friedmann, P. B. Mirkarimi, R. Pez, M. J. Mills, and K. F. McCarty, J. Appl. Phys. **76**, 295 (1994).

[30] P. B. Mirkarimi, K. F. McCarty, D. L. Medlin, W. G. Wolfer, T. A. Friedmann, E. J. Klaus, G. F. Cardinale, and D. G. Howitt, J. Mater. Res. **9**, 2925 (1994).

[31] W. Dworshak, K. Jung, and H. Ehrhardt, Thin Solid Films **254**, 65 (1995).

[32] D. J. Kester, K. S. Ailey, D. J. Lichtenwalner, and R. F. Davis, J. Vac. Sci. Technol. A **12**, 3074 (1994).

[33] K. G. Tirsell and V. Karpenko, Nucl. Instrum. Methods Phys. Res. Sect. A **291**, 511 (1990).

[34] D. G. J. Sutherland, H. Akatsu, M. Copel, F. J. Himpsel, T. A. Callcot, J. A. Carlisle, D. L. Ederer, J. J. Jia, I. Jimenez, R. Perera, D. K. Shuh, L. J. Terminello, and W. M. Tong, J. Appl. Phys. **78**, 6761 (1995).

[35] D. R. Strongin, J. K. Mowlem, M. W. Ruckman, and M. Strongin, Appl. Phys. Lett. **60**, 2561 (1992).

[36] J. F. Morar, F. J. Himpsel, G. Hollinger, G. Hughes, and J. L. Jordan, Phys. Rev. Lett. **54**, 1960 (1985).

[37] S. Shin, A. Agui, M. Fujisawa, Y. Tezuka, T. Ishii, Y. Minagawa, Y. Suda, A. Ebina, O. Mishina, and K. Era, Phys. Rev. B **52**, 11 853 (1995).

[38] V. Stambouli, O. Burat, D. Bouchier, and G. Gautherin, Surf. Coat. Technol. **43/44**, 137 (1990).

[39] G. Doll *et al.* (unpublished).

[40] H. Saitoh, K. Yoshida, and W. Yarbrough, J. Mater. Res. **8**, 8 (1993).

[41] H. Herchen and M. A. Cappelli, Phys. Rev. B **47**, 14 193 (1993); J. Liu, Y. K. Vohra, J. T. Tarvin, and S. S. Vagarali, *ibid.* **51**, 8591 (1995).

[42] J. Stöhr, *NEXAFS Spectroscopy* (Springer, Berlin, 1992).

[43] A. Chaiken, L. J. Terminello, J. Wong, G. L. Doll, and C. A. Taylor, Appl. Phys. Lett. **63**, 2112 (1993).

[44] D. J. Kesker, K. S. Ailey, R. F. Davis, and K. L. More, J. Mater. Res. **8**, 1213 (1993).